

# Empirical Estimates of Martian Surface Pressure in Support of the Landing of Mars Science Laboratory

Paul Withers

Received: 19 August 2011 / Accepted: 14 March 2012 / Published online: 31 March 2012  
© Springer Science+Business Media B.V. 2012

**Abstract** The aim of this work is to develop an empirical expression for diurnal mean martian surface pressure in support of the landing of Mars Science Laboratory. We evaluate the consistency of surface pressure measurements from four landers, Viking Lander 1, Viking Lander 2, Mars Pathfinder, and Phoenix, and one radio occultation experiment, Mars Global Surveyor. With the exception of Mars Pathfinder, whose measurements are 0.1 mbar smaller than expected, all are consistent. We assume that the diurnal mean surface pressure is a separable function of altitude and season, neglecting dependences on time of day, latitude, and longitude, and use the Viking Lander 1 dataset to characterize the seasonal dependence as a harmonic function of season with annual and semi-annual periods. We characterize the exponential dependence of surface pressure on altitude using Mars Global Surveyor radio occultation measurements widely-distributed below +1 km altitude and within 45 degrees of the equator. These measurements have local times of 3–5 hours, which may introduce biases into our estimates for diurnal mean surface pressure. Our empirical expression for diurnal mean surface pressure,  $p_{dm}$ , is  $p_{0,V L1} \exp(-(z - z_{0,V L1})/H_0) (1 + s_{1,V L1} \sin(1L_s) + c_{1,V L1} \cos(1L_s) + s_{2,V L1} \sin(2L_s) + c_{2,V L1} \cos(2L_s))$  where  $z$  is altitude,  $L_s$  is season, the reference pressure,  $p_{0,V L1}$ , is 7.972 mbar, the altitude of Viking Lander 1,  $z_{0,V L1}$ , is -3.63 km, the reference scale height,  $H_0$ , is 11 km, and the harmonic coefficients are  $s_1 = -0.069$ ,  $c_1 = 0.060$ ,  $s_2 = 0.045$ , and  $c_2 = -0.050$ . We validate this expression against the available datasets and estimate, with a 1- $\sigma$  confidence level of 2 %, a diurnal mean surface pressure of 7.30 mbar at Gale Crater, the Mars Science Laboratory landing site, at  $L_s = 150^\circ$ .

**Keywords** Mars, atmosphere · Atmospheres, structure

## 1 Introduction

The design of a spacecraft, such as NASA's Mars Science Laboratory (MSL), that will land on a planetary surface is influenced by the anticipated conditions in the corresponding plan-

---

P. Withers (✉)

Astronomy Department, Boston University, 725 Commonwealth Avenue, Boston, MA 02215, USA  
e-mail: [witthers@bu.edu](mailto:witthers@bu.edu)

etary atmosphere for the time and place at which the spacecraft will land. The likelihood of a safe landing increases as the difference between anticipated and actual conditions decreases. Long-range atmospheric estimates (climate) made prior to launch influence the spacecraft's hardware and software. Short-range atmospheric estimates (weather) made just before atmospheric entry can lead to modification of the software that controls the spacecraft during landing if deemed to increase the probability of a safe landing. In particular, the estimated surface pressure, which relates to the mass of the atmospheric column above the landing site, and the estimated vertical distribution of atmospheric mass have substantial influence on spacecraft design (Crisp et al. 2003).

From an atmospheric science perspective, the fundamental vertical structure is the variation of temperature with pressure, and this is what is most typically simulated or observed, whereas engineering applications focus on the variation of density with altitude, which is what impacts spacecraft survivability. These two viewpoints are linked by the equation of hydrostatic equilibrium, which requires a boundary condition. If surface pressure, the boundary condition, is poorly known, then the value of atmospheric science temperature-pressure information for mission planners is degraded. This was illustrated by an examination of the many predictions made for the Mars Exploration Rover (MER) landings (Withers et al. 2008). Predicted temperature-pressure profiles from a range of models were highly similar, but substantial differences existed in the corresponding density-altitude profiles that were traced to differences in the surface pressures.

The surface pressure of an atmosphere is the weight per unit area of the gas in the atmosphere (Chamberlain and Hunten 1987). For Mars, this approximately equals the product of the mass per unit area in the atmospheric column and the gravitational acceleration at the surface. The surface pressure at a particular location therefore depends on the total atmospheric mass and on how that mass is distributed across the planet. Indeed, the surface pressure can, in many cases, be considered to be proportional to the total atmospheric mass. The question of whether the total atmospheric mass is constant on decadal timescales is currently hotly debated and the answer has tremendous implications for understanding the future, recent, and distant climate of Mars (James et al. 1992; Tillman et al. 1993; Hinson 2003; Haberle and Kahre 2010). Mars is particularly unusual in that the total mass of its atmosphere changes significantly with season. "As much as 30 % of the atmosphere" cycles between gaseous and solid phases as  $\text{CO}_2$ , the most abundant atmospheric constituent, condenses in the winter polar night and sublimates in spring and summer (James et al. 1992). Consequently, surface pressure at a fixed location on Mars varies in phase with the total atmospheric mass over the course of a Mars year (Zurek et al. 1992, and references therein).

The surface pressure at fixed season varies with location, primarily due to variations in surface elevation (Zurek et al. 1992). Pressure decreases exponentially with altitude, and the range of surface elevations on Mars exceeds two scale heights (Smith et al. 2001). Indeed, surface pressure depends so strongly on altitude that the first topographic maps of Mars used surface pressure variations from Mariner 9 IRIS and radio occultation measurements as constraints. Surface pressure also depends, but to a lesser degree, on time of day, latitude and longitude due to atmospheric tides, Coriolis and centrifugal forces, and weather systems (e.g., Hess et al. 1980; Barnes 1981; Holton 1992; Tillman et al. 1993, 1994; Haberle et al. 1999; Hinson et al. 1999).

Variations in martian atmospheric mass with season and in the range of martian surface elevations relative to typical atmospheric scale heights are much greater than those that have been seen to date on Venus, Earth, Titan and Triton. Consequently, observed temporal and spatial variations in surface pressure on Mars are significantly greater than on those solar system bodies. The only other solid system body known to have a fluid atmosphere and

solid surface, Pluto, exhibits even greater variations in atmospheric mass. “Pressure at a given radius [on Pluto] approximately doubled between 1988 and 2002” (Elliot et al. 2007). Models suggest that Pluto’s atmosphere will fully condense for an appreciable fraction of its orbital period (Spencer et al. 1997).

The aim of the work reported herein is to develop, evaluate, and apply an empirical method for estimating martian surface pressure at the place and time of MSL’s landing. Despite this specificity to MSL, we also desire that our method gives reasonable results for a broader range of places and times so that it can be applied to projects more diverse than just the safe landing of MSL. Several highly-sophisticated physics-based models of Mars climate exist that can assimilate or otherwise use observations from different places and times to estimate conditions for MSL’s landing (Forget et al. 1999; Haberle et al. 1999; Lewis et al. 1999; Rafkin et al. 2001). Nevertheless, an estimate from a simple empirical model still possesses value. It can be evaluated without any consideration of whether the physics-based models contain the right physics, right boundary conditions, and right values of other inputs, let alone whether the code is 100 % bug-free. A simple empirical model can also provide estimates for any place and time without needing to initiate a time-consuming simulation. Finally, by being so close to the observational constraints, it can serve as a sanity check on estimates that are much harder to trace directly to observations.

This work occurred in parallel with MSL site selection, so the location and season of landing were not known at its onset. Candidate MSL landing sites had to be below +1 km altitude and within 45 degrees of the equator. Seasonal constraints were similarly broad at first, with MSL landing between  $L_s = 120^\circ$  and  $150^\circ$  for a 2009 launch and  $L_s = 150^\circ$  and  $180^\circ$  for a 2011 launch. Accordingly, the empirical model developed in this work was optimized to perform adequately at these altitudes, latitudes, and seasons, rather than exclusively focusing on the now-known location and season of landing. Gale Crater has since been selected as the landing site. The landing is scheduled to occur on 6 August 2012,  $L_s = 151^\circ$ , and 15 hrs local time at  $4.49^\circ\text{N}$ ,  $137.42^\circ\text{E}$ , and  $-4.451$  km.

Martian seasons are described by  $L_s$ , the angle between the Mars-Sun line and the Mars-Sun line at spring equinox in the northern hemisphere, known as the areocentric longitude of the Sun.  $L_s = 0^\circ$ ,  $90^\circ$ ,  $180^\circ$  and  $270^\circ$  define the onset of northern spring, summer, autumn and winter, respectively. We adopt the convention that Mars Year 1 began at  $L_s = 0^\circ$  on 11 April 1955 (Clancy et al. 2000).

Section 2 describes the available measurements of surface pressure. Section 3 describes the development of our empirical model and Sect. 4 describes its validation. Section 5 presents diurnal mean surface pressure estimates for MSL’s landing and Sect. 6 highlights other operational and scientific applications of our empirical model. Section 7 reports our conclusions.

## 2 Available Measurements of Surface Pressure

Two types of instruments have measured surface pressures on Mars: pressure sensors on landers have made *in situ* measurements and radio occultation experiments on orbiters have made remote sensing measurements.

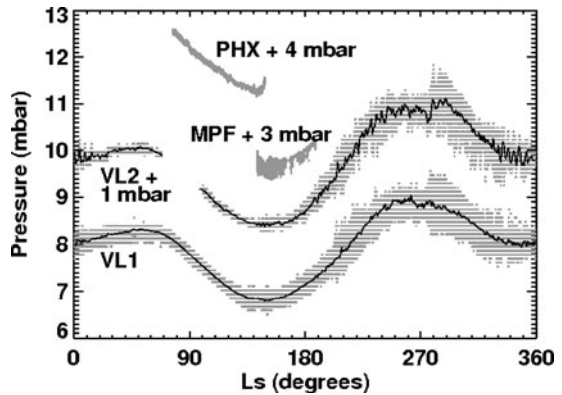
### 2.1 Landed Measurements of Surface Pressure

Landed measurements of surface pressure come from Viking 1 (VL1), Viking 2 (VL2), Pathfinder (MPF) and Phoenix (PHX) (Zurek et al. 1992; Haberle et al. 1999; Taylor et al.

**Table 1** Landed missions with pressure sensors. Locations for VL1, VL2 and MPF were obtained from Golombek et al. (2008) and the location for PHX was obtained from Golombek (personal communication, 2008). The remaining information was obtained from these instruments' PDS datasets and associated documentation

	VL1	VL2	MPF	PHX
Start date (UTC)	1976-07-20	1976-11-03	1997-07-04	2008-05-25
End date (UTC)	1982-11-05	1980-04-11	1997-09-27	2008-11-02
MY, $L_S$ at start date	12, 97°	12, 117°	23, 142°	29, 76°
MY, $L_S$ at end date	15, 221°	14, 91°	23, 188°	29, 151°
Altitude (km)	-3.63	-4.50	-3.68	-4.13
Latitude (°N)	22.27	47.62	19.09	68.22
Longitude (°E)	312.05	134.23	326.74	234.25
Number of measurements	89140	61389	453621	5556557

**Fig. 1** Surface pressure measurements (grey dots) from VL1, VL2, MPF and PHX as a function of season. Pressure offsets have been applied to several datasets to improve the clarity of this figure. Coarse digitization of the VL1 and VL2 measurements is apparent. The black lines through the VL1 and VL2 measurements indicate the diurnal mean surface pressure



2008). Pressure sensors were not flown on Spirit (SPI) and Opportunity (OPP) (Squyres et al. 2003). We now describe these landed measurements of surface pressure.

Each Viking lander carried a pressure sensor consisting of a “variable reluctance, stressed diaphragm” made of “thin stretched stainless steel” (Hess et al. 1977; Seiff 1976; Seiff and Kirk 1977). The accuracy of the sensors was  $\pm 0.01$  mbar, but digitization limited the resolution of their measurements to about 0.085 mbar. MPF carried “a Tavis deflecting diaphragm, variable reluctance sensor, similar to the Viking lander pressure sensors” (Seiff et al. 1997). The sensor’s 14 bit digitization provided 0.25 microbar resolution in its 6–10 mbar range and system noise levels were less than 2 counts ( $< 0.5$  microbar). The data used in this work were collected in the 6–10 mbar range. PHX carried three silicon diaphragm sensors, one of which was used as the prime sensor. “The pressure sensor is accurate to 10 Pa [0.1 mbar] between 7 and 11 hPa [7 and 11 mbar], and is sampled with 0.1 Pa [0.001 mbar] resolution” ([http://atmos.nmsu.edu/PDS/data/phmt\\_0001/CATALOG/MET\\_PT\\_INST.CAT](http://atmos.nmsu.edu/PDS/data/phmt_0001/CATALOG/MET_PT_INST.CAT)).

Surface pressures from the Viking, MPF, and PHX missions are archived at NASA’s Planetary Data System (PDS) and can be acquired from the Atmospheres Node. The locations and durations of these landed missions are listed in Table 1 and their surface pressure measurements are shown in Fig. 1. A strong seasonal variation in surface pressure is apparent in these datasets. The shape of the seasonal cycle appears to be similar in all four datasets, at least sufficiently similar for us to adopt as a starting point the premise that the surface

pressure equals  $P_0 f(L_s)$ , where  $P_0$  is a location-dependent reference pressure and  $f(L_s)$  is dimensionless. Subsequent sections will evaluate the accuracy of this premise.

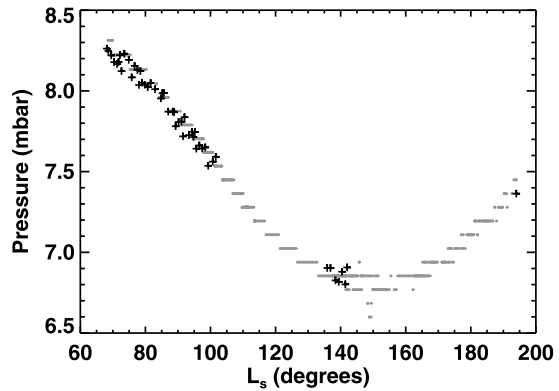
## 2.2 Orbital Measurements of Surface Pressure

Radio occultation measurements of surface pressure come from Mariner 9 (M9), Viking Orbiter 1 (VO1), Viking Orbiter 2 (VO2), Mars Global Surveyor (MGS) and Mars Express (MEX) (Zhang et al. 1990; Kliore 1992; Hinson et al. 1999, 2000; Pätzold et al. 2005). We now describe these orbital measurements of surface pressure.

Surface pressures obtained from the 260 successful radio occultations performed by M9 were reported in Kliore et al. (1972, 1973) and Kliore (1974). However, comparison of these measurements with other datasets suggests that the M9 surface pressures have errors of 10 % or greater, making them significantly less accurate than other available datasets. Hence M9 surface pressures are not used in this work. Approximately 20 surface pressure measurements from VO1 and VO2 have been published (Fjeldbo et al. 1977; Lindal et al. 1979), although many more radio occultation electron density profiles at ionospheric altitudes have been published (Zhang et al. 1990; Kliore 1992). Since there are so few of these Viking Orbiter measurements, they are not used in this work. The MGS radio occultation experiment has made 21243 neutral atmospheric profiles publicly available (Hinson et al. 1999, 2000). These are used extensively in this work. The MEX radio occultation experiment team has made 484 neutral atmospheric profiles available to us (Pätzold et al. 2004; Hinson et al. 2008a, 2008b). However, since only 5 MEX measurements are between  $L_s = 120^\circ$  and  $180^\circ$ , below +1 km altitude, and within 45 degrees of the equator, they are not used in this work (Hinson et al. 2008b).

Some additional processing was required in order to determine surface pressures from the archived MGS radio occultation pressure profiles. Radio occultation experiments determine atmospheric refractivity as a function of radial distance from time series of radio frequencies, as described by Hinson et al. (1999, and references therein). Neutral density is determined from refractivity using the known atmospheric composition, and pressure is determined from density using the equation of hydrostatic equilibrium and an upper boundary condition (Hinson et al. 1999). The resultant pressure profiles extend upwards from close to the surface until the atmosphere becomes too rarefied to produce significant refraction. The lower boundary of the pressure profiles is close to, but not perfectly at, the surface, so the pressure data point at the lowest altitude is not a true measure of the surface pressure. Accordingly, we used gridded MGS Mars Orbiter Laser Altimeter (MOLA) data products to determine the radius and altitude of the surface at the latitude and longitude of the occultation, then determined the surface pressure from the pressure profile by extrapolation using the assumption that pressure depends exponentially on altitude. The scale height used to extrapolate a given measured pressure-radius profile to the MOLA-provided surface radius was obtained from the dependence of pressure on altitude in that particular profile. No information from other MGS profiles, other datasets, or from the results listed in subsequent sections of this paper was used. Of particular importance is that the assumed value of  $H_0$  (equation (1)) was not used to obtain MGS surface pressures. The lowest point in the MGS pressure-radius profiles was typically less than 1 km above the MOLA surface, so any errors in the scale height used for extrapolation, which is on the order of 10 km, will have minimal consequences. Gridded MOLA data products are publicly available in the PDS at <http://pds-geosciences.wustl.edu/missions/mgs/megdr.html>. The PDS's unique identifying label for this dataset is MGS-M-MOLA-5-MEGDR-L3-V1.0. We use grids with resolution of 16 pixels per degree. The topographic grid is identified as MEGT90N000EB.IMG and the areoid grid is identified as MEGA90N000EB.IMG.

**Fig. 2** Comparison of landed and orbital measurements of surface pressure at similar seasons, LSTs, latitudes and longitudes for VL1 and MGS. Landed measurements are shown by *grey dots*. Orbital measurements are shown by *black crosses*. There are 573 landed measurements and 50 orbital measurements shown



### 2.3 Consistency of Different Datasets

It is important that we ensure that all datasets are consistent before using multiple datasets to develop our empirical model for surface pressure. In this section we compare the landed datasets to the MGS dataset. This implicitly assumes that interannual variability in surface pressure is negligible.

The comparison process for one landed dataset and the MGS dataset contains five steps. (1) Choose one landed dataset. (2) Retain only those MGS profiles whose season is within the range covered by the complete landed dataset, whose latitude is within 10 degrees of the lander's, and whose longitude is within 10 degrees of the lander's. In most cases, the retained MGS measurements have a narrow range (about 1 hr) of local solar times (LSTs). The exception is for PHX, where the MGS measurements have LST between 2 and 8 hrs. (3) Extrapolate all retained MGS pressure profiles to the lander's altitude (using the scale height implied by that MGS pressure profile). (4) Retain only those landed measurements whose season and LST are within the ranges covered by the retained MGS measurements. (5) Plot surface pressure as a function of season for retained landed and MGS measurements.

The process is slightly different for the MGS-MPF comparison as there are no MGS measurements near the MPF landing site during the seasonal range of the MPF mission. Instead, step 2 is modified to retain orbital profiles whose season is within  $10^\circ$  of the range covered by the complete landed dataset. Figures 2, 3, 4 and 5 show the results for comparison of MGS measurements to VL1, VL2, MPF, and PHX, respectively.

The MGS surface pressures are consistent with the VL1 and VL2 surface pressures, although the VL surface pressure measurements at fixed season and time of day vary over a range of about 0.2 mbar. The MGS surface pressures are consistent with the PHX surface pressures to significantly better than 0.1 mbar. The MGS surface pressures are systematically greater than the MPF surface pressures by about 0.1 mbar (1.5 %). The gain of the MPF pressure sensor was calibrated before the sensor was exposed to temperatures outside its design range during ground testing (Haberle et al. 1999), which might have changed its gain and which would account for this systematic difference in surface pressures (Schofield, 2008, personal communication). It is unlikely that either the MGS surface pressure dataset or interannual variability is responsible for this systematic difference given the similarity of MGS surface pressures to the VL1, VL2 and PHX measurements.

This section has established that MPF surface pressures seem 0.1 mbar too small and that VL1, VL2, PHX, and MGS surface pressures are self-consistent. It should be acknowledged that this conclusion for MPF is subject to the assumption that interannual variations

**Fig. 3** As Fig. 2, but for 3208 VL2 measurements and 75 MGS measurements

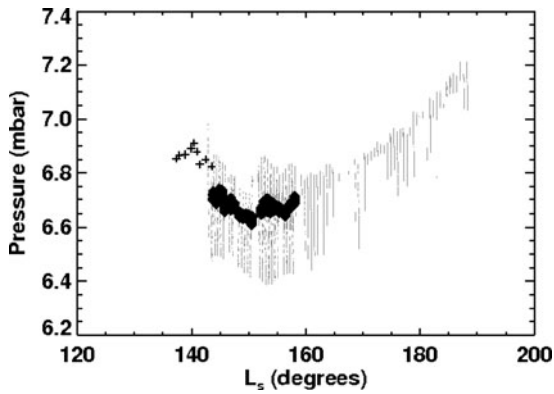
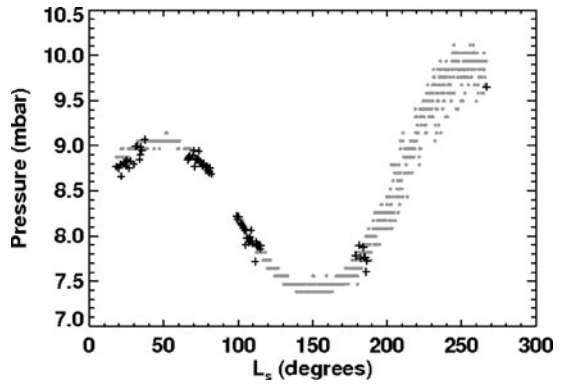
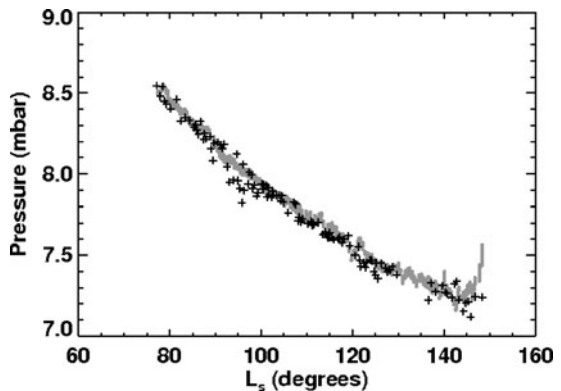


**Fig. 4** Comparison of landed and orbital measurements of surface pressure for MPF and MGS. *Grey dots* show all 453621 MPF surface pressure measurements. *Black crosses* show 9 MGS surface pressure measurements whose seasons are within  $10^\circ$  of the range covered by the complete MPF dataset, whose latitudes are within 10 degrees of the lander's, and whose longitudes are within 10 degrees of the lander's. The LST values of the plotted MGS surface pressures range from 4.1 to 4.3 hours. *Black diamonds* show 18875 MPF surface pressure measurements whose LSTs are between 3 and 5 hours, spanning the range of the MGS measurements. The differences between the MGS and MPF data indicate the presence of an offset in the MPF surface pressure measurements

**Fig. 5** As Fig. 2, but for 998422 PHX measurements and 120 MGS measurements



in surface pressure for its location and season are relatively small, which is a reasonable assumption. These self-consistent surface pressure measurements will now be utilized in Sects. 3 and 4 to develop and test an empirical expression for martian surface pressure.

### 3 Development of Empirical Expression for Surface Pressure

As discussed in Sect. 2, martian surface pressure varies significantly with season and altitude, so it is implausible that a useful expression could be found that does not depend on season or altitude. Surface pressure at a fixed location does vary with time of day, and this variation is typically repeatable from sol to sol (Tillman 1988; Haberle et al. 1999). The four landed datasets show that the root-mean-square of the difference between the surface pressure at fixed location and season and its diurnal mean value is typically on the order of 0.1 mbar, or about 1 % of the diurnal mean value (Tillman 1988; Haberle et al. 1999). However, the amplitudes and phases of the dominant harmonics in this diurnal cycle change with season and position, and their changes are not easily expressed by simple formulae. Variations in surface pressure with latitude or longitude are also complex (e.g., Hess et al. 1980; Barnes 1981; Holton 1992; Tillman et al. 1993, 1994; Haberle et al. 1999; Hinson et al. 1999). Therefore we searched for simple expressions for surface pressure that depend only on season and altitude. Given the challenges inherent in representing local time variations in surface pressure, we aimed to estimate diurnal mean surface pressures accurately, rather than at the precise local time of landing. This fact should be borne in mind when observations from a particular local time are compared against our estimates of diurnal mean conditions.

We first assume that diurnal mean surface pressure,  $p_{dm}$ , is a separable function of season and altitude, that the seasonal dependence is a harmonic series, and that the dependence on altitude,  $z$ , is exponential.

$$p_{dm} = p_0 \exp(-(z - z_0)/H_0) \left( 1 + \sum_{i=1}^n (s_i \sin(iL_s) + c_i \cos(iL_s)) \right) \quad (1)$$

The parameters of this model are  $p_0$ , a reference pressure,  $z_0$ , a reference altitude,  $H_0$ , a constant and uniform scale height, and the dimensionless harmonic coefficients,  $s_i$  and  $c_i$ . The harmonic series is truncated by  $n$ , and we refer to such a series as a “wave- $n$ ” series. This representation has several consequences for the implicitly assumed meteorology of Mars. It states that a given pressure level occurs at the same altitude at all locations and all seasons, which implies that dynamic meteorology is neglected. Yet lower atmospheric temperatures vary significantly with time of day and latitude, which should cause variations in the altitude at which a given pressure level occurs. Conveniently, near-surface atmospheric temperatures on Mars are only weakly dependent on altitude, relative to Earth, which makes these variations sufficiently small for the above expression to have a chance of being usefully accurate. One particularly valuable test of the accuracy of these assumptions is reported in Sect. 4 using a VL1–VL2 comparison. Our approach to using (1) is first to find  $p_0$  and the harmonic coefficients from landed datasets, then find  $H_0$  from the MGS dataset.

The best landed dataset to use to find  $p_0$  and the harmonic coefficients is VL1. VL1 and VL2 lasted for more than a full Mars year, whereas MPF and PHX lasted less than one quarter of a Mars year. VL2 did not measure surface pressure between  $L_s = 68^\circ$  and  $98^\circ$ , and its measurements are more disturbed by “traveling planetary waves, similar to mid-latitude storm systems on Earth” than those of VL1 (Zurek et al. 1992). Also, VL2 is lower in altitude and further north than candidate MSL landing sites, whereas VL1’s altitude and latitude are comparable to those of candidate MSL landing sites (Table 1).

**Fig. 6** The grey line shows diurnal mean surface pressures ( $p_{dm}$ ) for VL1 as a function of season. The black line shows the best fit to the grey line for a wave-2 series

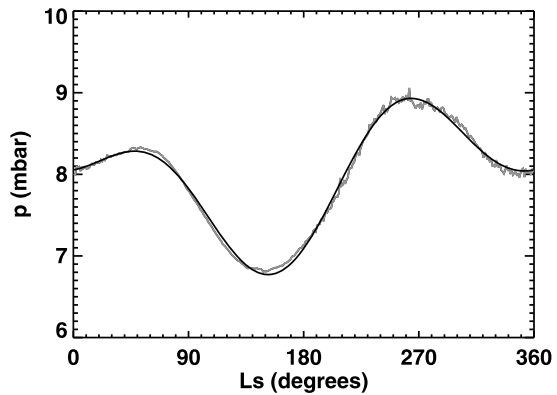


**Table 2** Parameters in the wave-2 series fit to diurnal mean surface pressures for Viking Lander 1 (equation (3))

Parameter	VL1 value
$p_0$ (mbar)	7.972
$s_1$	-0.069
$c_1$	0.060
$s_2$	0.045
$c_2$	-0.050

We first calculate diurnal mean surface pressures from the VL1 measurements. We assign each measurement to a bin based on its season,  $L_s = 0^\circ-1^\circ, 1^\circ-2^\circ, 2^\circ-3^\circ$ , etc. We fit the pressure measurements,  $p$ , in each  $L_s$  bin to a wave-4 harmonic series in LST:

$$p(x) = p_{dm} (1 + s_1 \sin(1x) + c_1 \cos(1x) + \dots + s_4 \sin(4x) + c_4 \cos(4x)) \quad (2)$$

where  $p_{dm}$  is the diurnal mean pressure and  $x$  is  $360^\circ \times \text{LST}/(24 \text{ hours})$ . The fitted values of  $p_{dm}$  form a smooth curve as a function of season, as shown in Fig. 6 (grey line).

Having obtained a set of 360 values of diurnal mean surface pressure that spans all seasons, thereby removing local time variations and the diurnal pressure cycle from consideration, we next represent the seasonal variation of diurnal mean surface pressure. We fit the function  $p_{dm}(L_s)$  to a wave-2 harmonic series and report the coefficients in Table 2. The fit is also shown in Fig. 6 (black line). The coefficients of higher order terms are an order of magnitude smaller, so we do not include them. Results are broadly similar to those of previous workers (e.g., Tillman et al. 1993). The root-mean-square difference between the 360 values of  $p_{dm}(L_s)$  found by averaging observations and the corresponding fitted values is 0.049 mbar, or 0.6 % of  $p_0$ . It is noteworthy that MSL will land at the minimum of the annual pressure cycle, even though small surface pressures make landing harder.

Given these values of  $p_0$  and the harmonic coefficients, we use the MGS dataset to find  $H_0$ . Based on the range of possible MSL landing sites and seasons at the time this work was conducted, we seek to optimize the estimates for  $L_s = 120^\circ$  and  $180^\circ$ , for altitudes below +1 km, and for latitudes within 45 degrees of the equator, subject to the constraint that the estimates are reasonably accurate for all seasons, altitudes and latitudes. Gale Crater has since been selected as the landing site. The landing is scheduled to occur on 6 August 2012,  $L_s = 151^\circ$ , 15 hrs local time at  $4.49^\circ\text{N}$ ,  $137.42^\circ\text{E}$ , and  $-4.451$  km. We define a metric,  $\Delta$ , as  $(p_{pred} - p_{meas})/p_{meas}$ , where  $p_{meas}$  is a pressure measurement and  $p_{pred}$  is the corresponding estimate. Acceptable values of  $H_0$  result in small absolute values of  $\Delta$ .

**Fig. 7** The dependence of  $\Delta$  on altitude for three selected values of  $H_0$  (10, 11, and 12 km). The observations are all 21243 MGS measurements. Values of  $\Delta$  for  $H_0$  equals 11 km and 12 km have been offset by 1 and 2, respectively. Horizontal lines mark  $\Delta = 0$  for each instance

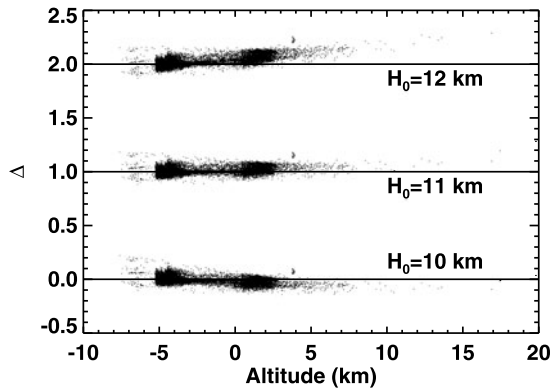
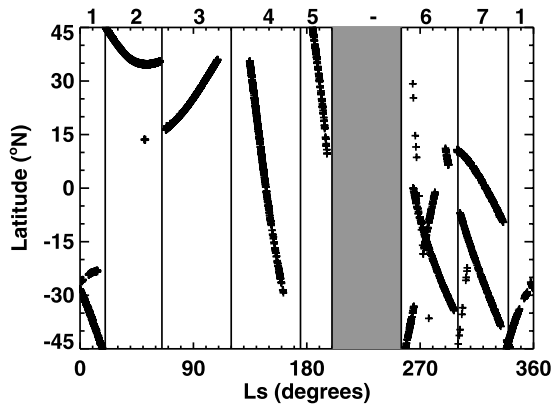


**Fig. 8** Crosses show 3069 MGS measurements that are below +1 km altitude and within 45° of the equator. They are divided by vertical lines into seven seasonal blocks, which are numbered. There are no crosses in the grey, unnumbered block between  $L_s = 200^\circ$  and  $L_s = 255^\circ$



We focus first on the complete MGS dataset. We select several trial value of  $H_0$  (10, 11, and 12 km) and find how  $\Delta$  depends on altitude. Results are illustrated in Fig. 7. On such a figure, a good value of  $H_0$  produces a cluster of points that appear independent of altitude and generally have small absolute values. Conversely, clusters of points that would be well fit by a sloping straight line exhibit unwanted dependence of  $\Delta$  on altitude and indicate a poor choice of  $H_0$ . Figure 7 shows that if  $H_0$  equals 10 km or less, then  $\Delta$  has a marked dependence on altitude, with large positive values of  $\Delta$  occurring at low altitudes. Figure 7 shows that if  $H_0$  equals 12 km or greater, then  $\Delta$  has a marked dependence on altitude, with large positive values of  $\Delta$  occurring at high altitudes. Since we ask that estimates be reasonably accurate under all conditions, the most promising range of potential  $H_0$  values is between 10 and 12 km.

The seasons and latitudes of the 3069 MGS measurements that are at altitudes below +1 km and within 45 degrees of the equator are shown in Fig. 8. They can be neatly divided into seven seasonal blocks, as indicated on Fig. 8. Table 3 lists the mean and standard deviation of  $\Delta$  for these seven blocks of measurements and for values of  $H_0$  between 10 and 15 km. The suggestion that  $H_0$  lies between 10 and 12 km arises from Fig. 7, which includes all 21243 MGS observations. Many of these come from high latitudes, which might bias our findings to small values of  $H_0$  that imply temperatures that might be considered unreasonably cold for the tropics. In nearly all of the seven seasonal blocks listed in Table 3, the estimates are worse (large absolute values of the mean of  $\Delta$  and large standard deviations

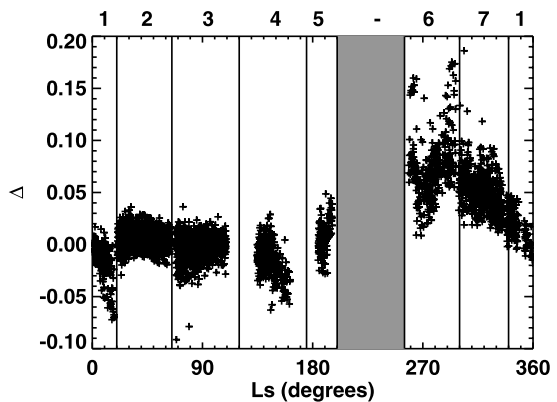
**Table 3** Dependence of  $\Delta$  on  $H_0$  as a function of season for MGS measurements below +1 km altitude and within 45 degrees of the equator.  $N$  is the number of MGS measurements that satisfy the altitude/latitude constraints and are within the stated seasonal range,  $\bar{z}$  is the mean altitude of these measurements,  $\bar{\Delta}$  is the mean value of  $\Delta$ , and S.D. of  $\Delta$  is the standard deviation of  $\Delta$ . Read  $-2.0E-02$  as  $-2.0 \times 10^{-2}$

$L_s$ range	$N$	$\bar{z}$ (km)	$H_0$ (km)	$\bar{\Delta}$	S.D. of $\Delta$
340°–20°	291	–1.3	10.0	–2.0E–02	3.2E–02
			10.5	–9.7E–03	2.5E–02
			11.0	3.2E–04	2.3E–02
			11.5	9.7E–03	2.6E–02
			12.0	1.8E–02	3.2E–02
			13.0	3.4E–02	4.5E–02
			14.0	4.8E–02	5.9E–02
20°–65°	824	–2.9	10.0	–4.2E–03	1.5E–02
			10.5	–8.7E–04	1.0E–02
			11.0	2.2E–03	1.0E–02
			11.5	5.0E–03	1.4E–02
			12.0	7.7E–03	1.8E–02
			13.0	1.2E–02	2.8E–02
			14.0	1.7E–02	3.7E–02
65°–120°	740	–2.2	10.0	–1.4E–02	1.9E–02
			10.5	–7.2E–03	1.5E–02
			11.0	–1.1E–03	1.4E–02
			11.5	4.6E–03	1.6E–02
			12.0	9.9E–03	1.9E–02
			13.0	1.9E–02	2.8E–02
			14.0	2.8E–02	3.6E–02
120°–175°	299	–1.7	10.0	–3.4E–02	2.6E–02
			10.5	–2.5E–02	2.1E–02
			11.0	–1.7E–02	1.8E–02
			11.5	–9.9E–03	1.7E–02
			12.0	–3.0E–03	1.8E–02
			13.0	9.4E–03	2.4E–02
			14.0	2.0E–02	3.1E–02
175°–200°	126	–2.8	10.0	1.4E–04	1.9E–02
			10.5	4.0E–03	1.6E–02
			11.0	7.5E–03	1.6E–02
			11.5	1.1E–02	1.8E–02
			12.0	1.4E–02	2.1E–02
			13.0	1.9E–02	2.9E–02
			14.0	2.4E–02	3.7E–02
			15.0	2.9E–02	4.5E–02

**Table 3** (Continued)

$L_s$ range	$N$	$\bar{z}$ (km)	$H_0$ (km)	$\bar{\Delta}$	S.D. of $\Delta$
255°–300°	311	−1.0	10.0	4.8E−02	4.4E−02
			10.5	6.1E−02	3.7E−02
			11.0	7.3E−02	3.1E−02
			11.5	8.4E−02	2.8E−02
			12.0	9.4E−02	2.7E−02
			13.0	1.1E−01	3.1E−02
			14.0	1.3E−01	3.8E−02
			15.0	1.4E−01	4.5E−02
300°–340°	478	−1.3	10.0	2.6E−02	2.9E−02
			10.5	3.8E−02	2.3E−02
			11.0	4.8E−02	2.0E−02
			11.5	5.8E−02	2.0E−02
			12.0	6.7E−02	2.3E−02
			13.0	8.3E−02	3.1E−02
			14.0	9.7E−02	4.1E−02
			15.0	1.1E−01	4.9E−02

**Fig. 9** Crosses show values of  $\Delta$  as a function of season. The observations are 3069 MGS measurements that are below +1 km altitude and within 45° of the equator. The measurements are divided into seven seasonal blocks as in Fig. 8



of  $\Delta$ ) for  $H_0 = 13\text{--}15$  km than for  $H_0 = 11$  km. Thus we can focus our attention on the  $H_0 = 10\text{--}12$  km range.

It is also apparent from Table 3 that the estimates are worse (large absolute values of the mean of  $\Delta$  and large standard deviations of  $\Delta$ ) for  $H_0 = 10$  km and  $H_0 = 12$  km than for the three intermediate scale heights. We therefore focus on the three intermediate scale heights, 10.5 km, 11.0 km and 11.5 km. For each of the seven seasonal blocks, the worst of these three estimates comes from either the 10.5 km scale height or the 11.5 km scale height—never the 11.0 km scale height. Estimates using the 11.0 km scale height are reasonable for the  $L_s = 120^\circ$  to  $175^\circ$  and  $L_s = 175^\circ$  to  $200^\circ$  seasonal blocks that are most important for MSL. Therefore we adopt  $H_0 = 11$  km and show the resultant values of  $\Delta$  in Fig. 9. This scale height corresponds to a temperature of about 215 K, which is reasonable (Seiff and Kirk 1977; Smith 2004, 2008). The MGS measurements used to find  $H_0 = 11$  km have

strongly biased local time coverage. The implications of this sampling bias for estimates of diurnal mean surface pressure are discussed in Sect. 4.

Figure 9 shows that absolute values of  $\Delta$  are significantly larger for  $L_s = 255^\circ$  to  $340^\circ$  than for  $L_s = 340^\circ$  to  $360^\circ/0^\circ$  to  $200^\circ$ , which corresponds to seasons when dust storms are most likely to increase atmospheric variability planet-wide and when traveling planetary waves increased atmospheric variability at the two Viking landing sites (particularly the more northern VL2 site) (Zurek et al. 1992).

Our empirical expression for martian surface pressure is:

$$p_s = p_{0,VL1} \exp(-(z - z_{0,VL1})/H_0) \times (1 + s_{1,VL1} \sin(1L_s) + c_{1,VL1} \cos(1L_s) + s_{2,VL1} \sin(2L_s) + c_{2,VL1} \cos(2L_s)) \quad (3)$$

where the values of  $p_0$ ,  $s_1$ ,  $c_1$ ,  $s_2$  and  $c_2$  are the VL1 values in Table 2, the value of  $z_{0,VL1}$ , the altitude of Viking Lander 1, is given in Table 1, and  $H_0$  is 11 km.

### 4 Validation of Empirical Expression for Surface Pressure

We now test our empirical expression using the VL1, VL2, MPF, PHX, and MGS datasets.

Figure 10 shows  $\Delta$  for VL1, which is independent of  $H_0$ . For the 360 values of  $p_{dm}$  obtained from VL1, the mean of  $\Delta$  is  $2.5 \times 10^{-3}$  percent and the standard deviation of  $\Delta$  is 0.6 %. For the 60 values of  $p_{dm}$  obtained from VL1 between  $L_s = 120^\circ$  and  $180^\circ$ , the mean of  $\Delta$  is  $-0.4$  % and the standard deviation of  $\Delta$  is 0.6 %. Such excellent estimates are not surprising, since our empirical expression was based on VL1 data. The non-zero standard deviations simply reflect higher frequency oscillations than are represented in the wave-2 fit to the VL1 data.

Diurnal mean surface pressures were obtained from the VL2 dataset as a function of season,  $p_{dm}(L_s)$ , at one degree intervals using the technique applied previously to VL1. Results are shown in Fig. 11. Values of  $\Delta$  were found for the observed  $p_{dm}(L_s)$ , as shown in Fig. 12. The estimates were least accurate during northern autumn and winter, as expected given the elevated atmospheric variability at these seasons (Zurek et al. 1992). For the 331 values of  $p_{dm}$  obtained from VL2, the mean of  $\Delta$  is  $6.7 \times 10^{-3}$  percent and the standard deviation of  $\Delta$  is 1.1 %. For the 60 values of  $p_{dm}$  obtained from VL2 between  $L_s = 120^\circ$  and  $180^\circ$ , the mean of  $\Delta$  is  $-0.4$  % and the standard deviation of  $\Delta$  is 0.6 %. Figure 13 shows that the atmospheric scale height implied by the difference between the VL1 and VL2 surface pressures varies strongly with season between 6 km and 13 km. The small

**Fig. 10** Crosses show values of  $\Delta$  as a function of season for 360 diurnal mean surface pressures,  $p_{dm}$ , from VL1

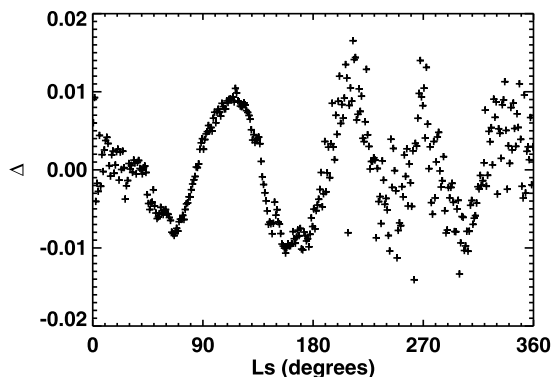


**Fig. 11** As Fig. 6, but for VL2

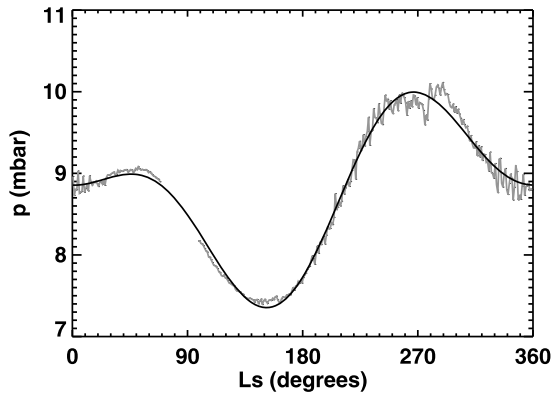


**Fig. 12** Crosses show values of  $\Delta$  as a function of season for 331 diurnal mean surface pressures,  $p_{dm}$ , from VL2

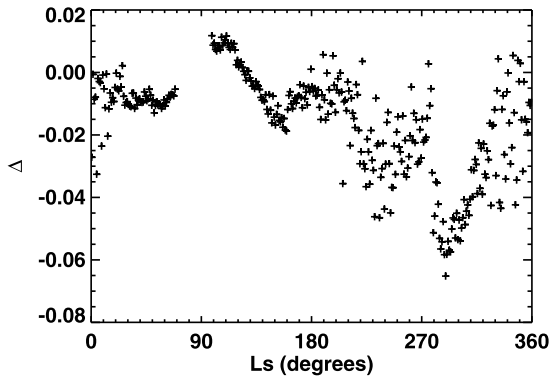
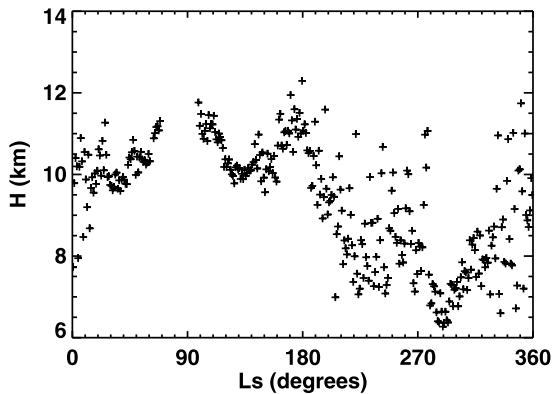
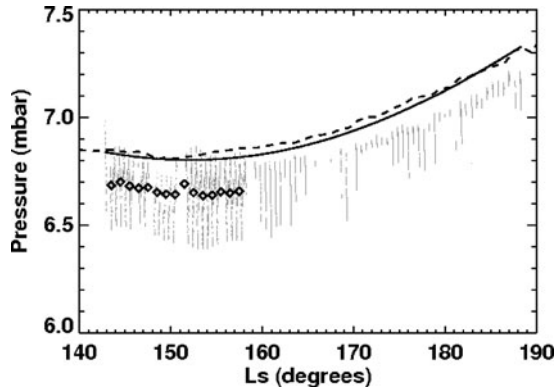


**Fig. 13** Crosses show the atmospheric scale height implied by the difference between the diurnal mean surface pressures from VL1 and VL2. It is calculated as  $-(z_{0,VL1} - z_{0,VL2}) / \ln(p_{dm,VL1} / p_{dm,VL2})$

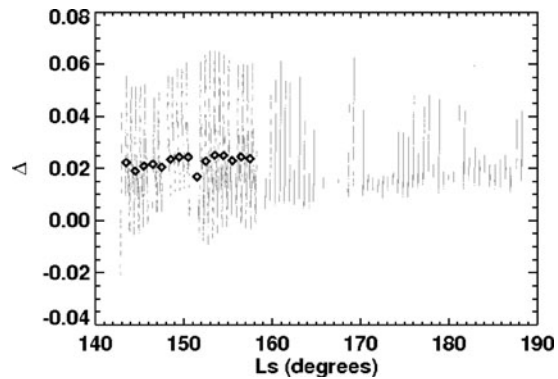


altitude difference between the VL1 and VL2 landing sites explains why estimated VL2 surface pressures found using a fixed scale height are nevertheless quite accurate (Figs. 11 and 12). It also means that values of  $H_0$  obtained from analysis of VL1–VL2 differences exaggerate the effects of minor changes in surface pressure. Indeed, one of the primary reasons for using the MGS dataset rather than the VL2 dataset to provide  $H_0$  is the vertical range covered by the distributed MGS measurements.

**Fig. 14** Grey dots show 453621 individual surface pressure measurements from MPF. Black diamonds show 15 diurnal mean surface pressures from MPF. The solid black line shows our estimated surface pressures for MPF. The dashed black line shows  $p_{dm}$  for VL1, which is only 50 m higher than MPF. The difference between the VL1 and MPF data indicate the presence of an offset in the MPF surface pressure measurements



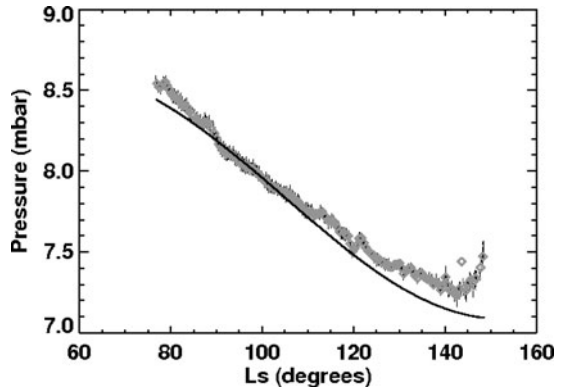
**Fig. 15** Grey dots show  $\Delta$  as a function of season for 453621 individual surface pressure measurements from MPF. Black diamonds show  $\Delta$  as a function of season for 15 measurements of diurnal mean surface pressures from MPF



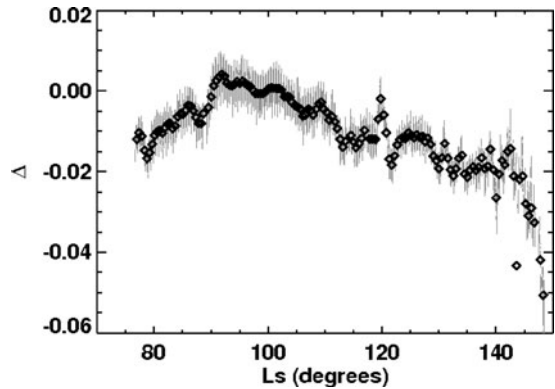
The estimates for MPF are not very sensitive to  $H_0$  since the altitudes of the VL1 and MPF landing sites differ by only 50 m (Table 1). Figure 14 shows individual surface pressure measurements for MPF, corresponding estimates, diurnal mean surface pressures for MPF, and diurnal mean surface pressures for VL1. Diurnal mean surface pressures for MPF were calculated in the same 1 degree bins used for VL1 and VL2, but could only be determined when observations were made over a wide range of LSTs. This only occurred at the beginning of the mission. The estimated pressures for MPF are systematically 0.15 mbar greater than the observed diurnal mean surface pressures, which is comparable to the 0.1 mbar systematic offset inferred in Sect. 2.3 from MGS-MPF comparisons. If MPF and VL1 diurnal mean surface pressures are compared directly, ignoring the small 50 m altitude difference, then the VL1 pressures are systematically greater than the MPF pressures. This difference is 0.15 mbar at  $L_s = 143^\circ$  and it increases to 0.20 mbar at  $L_s = 157^\circ$ . Figure 15 shows  $\Delta$  for MPF using both individual surface pressure measurements and diurnal mean surface pressures. For the 15 values of  $p_{dm}$  obtained from MPF, the mean of  $\Delta$  is 2.2 % and the standard deviation of  $\Delta$  is 0.2 %. The systematic error in the MPF surface pressure measurements greatly reduces the usefulness of this dataset for testing our expressions for surface pressure.

Figure 16 shows individual surface pressure measurements for PHX, corresponding estimates, and diurnal mean surface pressures for PHX. Due to the much higher frequency of PHX measurements relative to earlier landers, each diurnal mean surface pressure for PHX is obtained from a fit to one sol's data. The fitting function is the same as was used for earlier landers (equation (2)). Due to data gaps, no diurnal mean was calculated for the sol centered on  $L_s = 114.2^\circ$ . Figure 17 shows  $\Delta$  for PHX. For the 87 values of  $p_{dm}$  obtained from PHX,

**Fig. 16** Black dots show 5556557 individual surface pressure measurements from PHX. Grey diamonds show 148 diurnal mean surface pressures from PHX. The solid black line shows estimated surface pressures for PHX



**Fig. 17** Grey dots show  $\Delta$  as a function of season for 5556557 individual surface pressure measurements from PHX. Black diamonds show  $\Delta$  as a function of season for 148 measurements of diurnal mean surface pressures from PHX

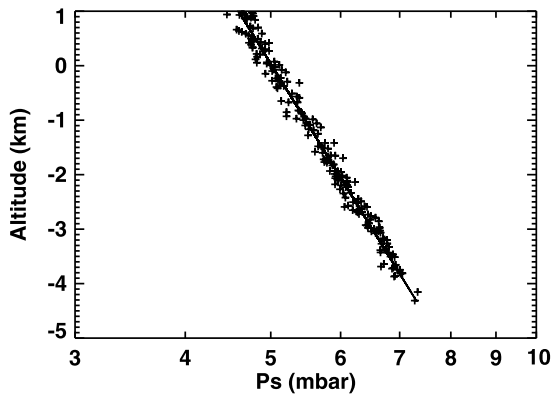


the mean of  $\Delta$  is  $-1.0\%$  and the standard deviation of  $\Delta$  is  $0.9\%$ . For the 56 values of  $p_{dm}$  obtained from PHX between  $L_s = 120^\circ$  and  $180^\circ$ , the mean of  $\Delta$  is  $-1.9\%$  and the standard deviation of  $\Delta$  is  $0.8\%$ .

Figure 9 shows  $\Delta$  for MGS. For the complete set of 21243 MGS measurements, the mean of  $\Delta$  is  $0.9\%$  and the standard deviation of  $\Delta$  is  $3.1\%$ . LSTs of the 21243 MGS measurements are, on the whole, between 3 and 15 hours. For the subset of 3069 MGS measurements that are below  $+1$  km altitude and within 45 degrees of the equator, the mean of  $\Delta$  is  $1.4\%$  and the standard deviation of  $\Delta$  is  $3.3\%$ . LSTs of this subset of 3069 MGS measurements are, on the whole, between 3 and 5 hours. For the subset of 299 MGS measurements that are between  $L_s = 120^\circ$  and  $180^\circ$ , below  $+1$  km altitude and within 45 degrees of the equator, the mean of  $\Delta$  is  $-1.7\%$  and the standard deviation of  $\Delta$  is  $1.8\%$ . LSTs of this subset of 299 MGS measurements are between 4.1 and 4.5 hours. Although the MGS measurements were used to develop the empirical expression for surface pressure, they were acquired at a range of altitudes, latitudes and longitudes—unlike the  $p_{dm}$  found for VL1. Thus they are still valuable for evaluating the accuracy of this empirical expression, even if they do not provide a completely independent perspective.

The concentration of MGS measurements in a narrow range of LSTs might be considered a problem when both developing and testing estimates of diurnal mean surface pressure. The 3069 MGS measurements that are below  $+1$  km altitude and within 45 degrees of the equator and that were used to obtain  $H_0 = 11$  km have local times that are predominantly between 3 and 5 hours. Does this bias towards the cold nighttime mean that the assumed

**Fig. 18** Crosses show all 198 MGS surface pressure measurements from  $L_s = 140^\circ\text{--}160^\circ$ , latitudes equatorward of 45 degrees, and altitudes below +1 km. Their local times are 4.1–4.4 hrs. The solid line shows an exponential fit to the data with a scale height of 11.6 km and a reference pressure at the VL1 altitude of 6.89 mbar



value of  $H_0$  is too small? The comparison between VL1 and VL2 diurnal mean surface pressures in Fig. 13 suggests  $H_0 = 11$  km is reasonable, except around  $L_s = 270^\circ$  when this figure favors a significantly smaller value of  $H_0$  (albeit from two sites whose proximity in altitude means that minor variations in meteorologic conditions can imply major changes in the inferred  $H_0$ ). In addition, tests in this section of estimated surface pressures using  $H_0 = 11$  km and direct observations of diurnal mean surface pressure from VL2, MPF, and PHX did not reveal any major weaknesses in the estimates.

Direct information on the scale of the diurnal pressure cycle comes from VL1 and VL2. The root-mean-square difference between the diurnally-varying Viking Lander surface pressures and the diurnal mean at  $L_s = 120^\circ\text{--}175^\circ$ , which contains the MSL landing interval, is 1.2 % for VL1 and 0.4 % for VL2, which are relatively small. Also, an estimate of  $H_0$  can be obtained from the MGS measurements alone, without any dependence on the VL1 data. Figure 18 shows all 198 MGS surface pressure measurements from  $L_s = 140^\circ\text{--}160^\circ$ , latitudes equatorward of 45 degrees, and altitudes below +1 km. They are well fit by an exponential dependence on altitude with a scale height of 11.6 km, close to the value of 11 km adopted for  $H_0$  in this work, and a reference pressure at the VL1 altitude of 6.89 mbar. The root-mean-square difference between the data and the fit is less than 2 %. The average diurnal mean surface pressure measured by VL1 for this range of seasons was 6.84 mbar, which differs by less than 1 % from the fitted value of 6.89 mbar. The available evidence indicates that  $H_0 = 11$  km is reasonable for the purposes of this paper, even though the local times of the constraining MGS measurements are strongly biased to between 3 and 5 hours.

The estimates of MGS surface pressures are least accurate in the  $L_s = 255^\circ\text{--}300^\circ$  seasonal block (Fig. 9). Several factors may account for this. Firstly, this is a season of high interannual variability on Mars. The MGS data span multiple Mars Years, all from the post-Viking epoch. Secondly, the comparison between VL1 and VL2 surface pressures in Fig. 13 shows that the assumption of a season-independent value of  $H_0$  is particularly weak at this season. Thirdly, atmospheric tides are enhanced at this season due to the increased abundance of suspended radiatively-active dust. Such enhancements increase the difference between the diurnal mean surface pressure and the surface pressure at a particular local time. Since the optimal value of  $H_0$  was found by comparison of VL1 diurnal mean surface pressures and MGS observations concentrated at a local time of 3–5 hours, the optimal value of 11 km found in Sect. 3 might be less accurate than usual for this season. Fourthly, the locations of the MGS data at this season are more weighted towards southern mid-latitudes than

**Table 4** Performance of our empirical expression. Observed diurnal mean surface pressures are used for the landed datasets. Only measurements below +1 km altitude and within 45 degrees of the equator are used for the MGS dataset

Mission	$\overline{\Delta}$ (all $L_s$ )	S.D. of $\Delta$ (all $L_s$ )	$\overline{\Delta}$ ( $L_s = 120^\circ\text{--}180^\circ$ )	S.D. of $\Delta$ ( $L_s = 120^\circ\text{--}180^\circ$ )
VL1	2.5E-3 %	0.6 %	-0.4 %	0.6 %
VL2	6.7E-3 %	1.1 %	-0.4 %	0.6 %
MPF	2.2 %	0.2 %	2.2 %	0.2 %
PHX	-1.0 %	0.9 %	-1.9 %	0.8 %
MGS	1.4 %	3.3 %	-1.7 %	1.8 %

at some other seasons, such as  $L_s = 20^\circ\text{--}200^\circ$ . However, the same is true for the  $L_s = 340^\circ\text{--}20^\circ$  seasonal block, where the estimated pressures are perfectly reasonable.

Table 4 summarizes the performance of our empirical expression. Results for VL2 and MGS are most relevant and results for VL1, MPF, and PHX are less relevant. Estimates for VL1 are essentially required to agree very well with the measurements. The MPF measurements were affected by a systematic error, which accounts for MPF’s large mean value of  $\Delta$ . PHX is much further poleward than possible MSL landing sites. Based on these results, we expect, at a 1 -  $\sigma$  confidence level, that the diurnal mean surface pressure estimated for the MSL landing by our empirical expression will be within 2 % of the actual value.

### 5 Estimates for MSL

Much of this work was performed at a time when there were four candidate landing sites for MSL. Their locations are listed in Table 5 and estimated diurnal mean surface pressures as functions of season are shown in Fig. 19. Numerical values of estimates at  $L_s = 120^\circ, 150^\circ$  and  $180^\circ$  are listed in Table 6.

One final type of observation should be mentioned here. The CRISM infrared spectrometer on Mars Reconnaissance Orbiter (MRO) retrieves surface pressure (Smith et al. 2009), albeit with estimated accuracies of 10 %. Fortuitously, MRO’s extensive observations of the MSL candidate landing sites led to its acquisition of one CRISM measurement of surface pressure at Gale Crater, the selected landing site, at close to the season and local time of landing. The surface pressure at 4.484°S, 137.405°E, 15.728 hrs LST,  $L_s = 151.323^\circ$  in MY 29 was 7.0 mbar (personal communication, M. Smith, 2010). The corresponding elevation is -4.439 km. Our estimate for the diurnal mean surface pressure at Gale Crater (-4.451 km) at  $L_s = 150^\circ$  is 7.30 mbar, 4 % greater than this observation. Given the observational uncertainty of 10 %, the estimate is entirely consistent with the CRISM observation. None of the other orbital datasets we inspected during the course of this project had measurements so close in location, season, and local time to potential landing conditions at any of the four candidate sites. MCS data were not inspected as uncertainties in its spacecraft pointing lead to uncertainties in the radius at which a particular pressure level occurs. These uncertainties in radius degrade the accuracy of surface pressures obtained by hydrostatic extrapolation.

One caveat should be emphasized again. The critical parameter  $H_0$  has been determined using MGS data biased to local times of 3–5 hours. Preceding sections have tested whether this bias introduces significant errors into estimates of diurnal mean surface pressure. We have found that the estimates appear reasonable given the data available to test them. However, the landed surface pressure measurements come from an altitude range less than 1 km

**Table 5** Locations of four candidate landing sites for MSL (Chen, personal communication, 2008)

Name	Altitude (km)	Latitude (°N)	Longitude (°E)
Eberswalde Crater	-1.450	-23.86	326.73
Gale Crater	-4.451	-04.49	137.42
Holden Crater Fan	-1.940	-26.37	325.10
Mawrth Vallis—Site 2	-2.246	24.01	341.03

**Fig. 19** Estimated diurnal mean surface pressure as a function of season for candidate MSL landing sites. Eberswalde Crater: *black solid line*, Gale Crater: *grey solid line*, Holden Crater Fan: *black dashed line*, Mawrth Vallis—Site 2: *grey dashed line*

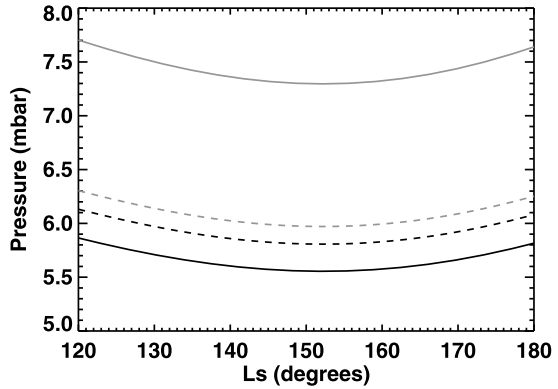


**Table 6** Estimated diurnal mean surface pressures at four candidate landing sites for MSL

Name	Season	$p_{dm}$ (mbar)
Eberswalde Crater	$L_s = 120^\circ$	5.86
	$L_s = 150^\circ$	5.56
	$L_s = 180^\circ$	5.82
Gale Crater	$L_s = 120^\circ$	7.70
	$L_s = 150^\circ$	7.30
	$L_s = 180^\circ$	7.64
Holden Crater Fan	$L_s = 120^\circ$	6.13
	$L_s = 150^\circ$	5.81
	$L_s = 180^\circ$	6.08
Mawrth Vallis—Site 2	$L_s = 120^\circ$	6.30
	$L_s = 150^\circ$	5.97
	$L_s = 180^\circ$	6.25

wide, which makes them of limited utility for testing  $H_0$ , and the only directly relevant orbital data (MGS) have biased local time sampling, so there are intrinsic limitations in the tests that can be performed using direct comparison to surface pressure observations. Since Gale Crater is at almost the same altitude as VL2, it might be instructive to note that the diurnal mean surface pressure for VL2 at  $L_s = 150^\circ$  is 7.45 mbar, 2 % larger than our estimate for Gale Crater. Meridional differences in meteorology, which are minimized in our estimates, may explain why the estimated surface pressure at Gale Crater differs from that observed at the VL2 site, despite their near-identical altitudes.

## 6 Other Applications

The operational implications of simple and accurate methods for estimating martian surface pressure extend beyond MSL. From an operational perspective, other mission design efforts can use the work reported here to make first-order estimates of surface pressure for candidate landing sites and times. They can also use it as a straight-forward “reality-check” on the predictions of more complex models.

There are also potential scientific applications, such as the determination of the total atmospheric mass. Variations in the total mass of the martian atmosphere with time are important for several research areas, including the martian rotational state (e.g. Defraigne et al. 2000; Van den Acker et al. 2002) and the martian gravitational field (e.g. Smith et al. 1999; Sanchez et al. 2006; Karatekin et al. 2006). The atmospheric mass per unit area is the surface pressure divided by the acceleration of gravity. From (1), the total atmospheric mass,  $M$ , satisfies:

$$M = \frac{p_0 f(L_s) R^2}{g} \int_{\phi=0}^{\phi=2\pi} \int_{\theta=0}^{\theta=\pi} \exp(-(z - z_0)/H_0) \sin \theta d\theta d\phi \quad (4)$$

where  $R$  is the planetary radius, 3400 km,  $g$  is the acceleration due to gravity,  $3.7 \text{ ms}^{-2}$ ,  $\theta$  is colatitude,  $\phi$  is longitude, and we have abbreviated the seasonal dependence to  $f(L_s)$  for convenience. If the entire planetary surface had an altitude of  $z_0$ , the numerical value of the integral in (4) would equal  $4\pi$ . Instead, using the 16 pixels per degree MOLA grid and  $H_0 = 11 \text{ km}$ , it equals 9.83 or 78 % of  $4\pi$ . The estimated mean total atmospheric mass is approximately  $2.4 \times 10^{16} \text{ kg}$ . The estimated difference between the maximum and minimum atmospheric mass is  $6.6 \times 10^{15} \text{ kg}$ , or 27 % of the mean atmospheric mass. If this mass difference were uniformly deposited in one hemisphere at latitudes poleward of  $75^\circ$  (or  $65^\circ$ ) with a density of  $910 \text{ kg m}^{-3}$  (Smith et al. 2001), then the resultant seasonal polar cap would have a height of 3 m (or 1 m). These estimates of total atmospheric mass, range in atmospheric mass, and seasonal elevation changes are broadly consistent with earlier publications (e.g., James et al. 1992; Zurek et al. 1992; Smith et al. 2001; Karatekin et al. 2006; Kelly et al. 2006), which builds confidence in our empirical expression. To the best of our knowledge, this is the first integration of Viking Lander-derived surface pressures across the MOLA areoid.

There is a smorgasbord of other scientific applications of knowledge of martian surface pressure, including dust lifting, aeolian modification of surface features, thermodynamic stability of near-surface liquids (McEwen et al. 2011), and the radiation environment at the surface. Martian surface pressure is important for accurate interpretation of Odyssey Gamma Ray Spectrometer (GRS) data as well (Boynton et al. 2004). Finally, knowledge of martian surface pressure can be used to estimate absolute altitude scales for atmospheric temperature-pressure profiles measured from orbit, including profiles from the Mariner 9 Infrared Interferometer Spectrometer (IRIS) and MGS TES instruments. The empirical expression developed and tested in this work can be considered for use in these areas alongside existing representations of surface pressure.

## 7 Conclusions

Surface pressure is a critical factor for the safe landing of spacecraft on the surface of Mars. Accurate estimates of surface pressure with accurately characterized uncertainties are required for the design of spacecraft hardware long before launch and for the optimization

of the landing control algorithm up to the day of landing itself. Straight-forward empirical models for surface pressure are valuable, despite the availability of predictions from sophisticated physics-based numerical models, because they can generate estimates instantly, have output that is closely connected and clearly traceable to observational constraints, and have readily-characterized uncertainties.

Our empirical expression for diurnal mean surface pressure on Mars, which consists of an exponential dependence on altitude and an annual and semi-annual dependence on season, has been validated satisfactorily. It reproduces diurnal mean surface pressure measurements for VL1, VL2, MPF, and PHX to an accuracy of  $\sim 2\%$ . It is slightly less accurate, but still adequate, at reproducing selected individual (not diurnal mean) MGS radio occultation measurements of surface pressure, which are widely-distributed below +1 km altitude and within 45 degrees of the equator. We estimate, with a  $1 - \sigma$  confidence level of  $2\%$ , a diurnal mean surface pressure of 7.30 mbar at Gale Crater, the MSL landing site, at  $L_s = 150^\circ$ . The major weakness in the development of this estimate is the limited local time coverage of relevant MGS measurements.

Although the development of this expression was focused on application to the safe landing of MSL, the expression is designed to fail gracefully when applied to different seasons or locations. Therefore it can be applied at all seasons to conditions as extreme as deep craters, high mountains, and polar terrain, albeit with performance that is as yet poorly characterized. MGS and other datasets could be used to characterize the accuracy of this expression at extreme altitudes. It is likely that the optimum expression would be somewhat different for studies focused on other altitudes. As expected, our empirical expression is least accurate at reproducing MGS radio occultation measurements at  $L_s = 255^\circ - 340^\circ$ , which encompasses the seasons when atmospheric conditions are perturbed by large and spatially- and temporally-variable quantities of suspended, radiatively-active dust (Smith 2008) (there are no MGS measurements at  $L_s = 200^\circ - 255^\circ$ ). Other possible operational applications of this expression include estimates for the landing and surface operations of future landers. Possible scientific applications of this expression include studies of the total atmospheric mass and its spatial and temporal variability, simulations of near-surface environmental conditions, and interpretation of observations.

**Acknowledgements** This work was stimulated by substantial differences between predicted atmospheric conditions for the MER landings, most of which could be traced to differences in simulated surface pressure. PW acknowledges two anonymous reviewers for helpful evaluations; Jere Justus, David Kass, Scot Rafkin and Luca Montabone for sharing their MER predictions; Martin Pätzold and the MaRS team for data from the Mars Express radio occultation experiment; Mike Smith for CRISM data; Allen Chen, Ashwin Vasavada, and the MSL Council of Atmospheres for discussions; and the NASA JPL Mars Critical Data Products Initiative for support via subcontract 1316618.

## References

- J.R. Barnes, Midlatitude disturbances in the Martian atmosphere—A second Mars year. *J. Atmos. Sci.* **38**, 225–234 (1981). doi:[10.1175/1520-0469\(1981\)038](https://doi.org/10.1175/1520-0469(1981)038)
- W.V. Boynton, W.C. Feldman, I.G. Mitrofanov, L.G. Evans, R.C. Reedy, S.W. Squyres, R. Starr, J.I. Trombka, C. D’Uston, J.R. Arnold, P.A.J. Englert, A.E. Metzger, H. Wänke, J. Brückner, D.M. Drake, C. Shinohara, C. Fellows, D.K. Hamara, K. Harshman, K. Kerry, C. Turner, M. Ward, H. Barthe, K.R. Fuller, S.A. Storms, G.W. Thornton, J.L. Longmire, M.L. Litvak, A.K. Ton’chev, The Mars Odyssey Gamma-Ray Spectrometer instrument suite. *Space Sci. Rev.* **110**, 37–83 (2004). doi:[10.1023/B:SPAC.0000021007.76126.15](https://doi.org/10.1023/B:SPAC.0000021007.76126.15)
- J.W. Chamberlain, D.M. Hunten, *Theory of Planetary Atmospheres*, 2nd edn. (Academic Press, New York, 1987)

- R.T. Clancy, B.J. Sandor, M.J. Wolff, P.R. Christensen, M.D. Smith, J.C. Pearl, B.J. Conrath, R.J. Wilson, An intercomparison of ground-based millimeter, MGS TES, and Viking atmospheric temperature measurements: Seasonal and interannual variability of temperatures and dust loading in the global Mars atmosphere. *J. Geophys. Res.* **105**, 9553–9572 (2000)
- J.A. Crisp, M. Adler, J.R. Matijevic, S.W. Squyres, R.E. Arvidson, D.M. Kass, Mars Exploration Rover mission. *J. Geophys. Res.* **108**, 8061 (2003). doi:[10.1029/2002JE002038](https://doi.org/10.1029/2002JE002038)
- P. Defraigne, O. de Viron, V. Dehant, T. Van Hoolst, F. Hourdin, Mars rotation variations induced by atmosphere and ice caps. *J. Geophys. Res.* **105**, 24563–24570 (2000). doi:[10.1029/1999JE001227](https://doi.org/10.1029/1999JE001227)
- J.L. Elliot, M.J. Person, A.A.S. Gulbis, S.P. Souza, E.R. Adams, B.A. Babcock, J.W. Gangestad, A.E. Jaskot, E.A. Kramer, J.M. Pasachoff, R.E. Pike, C.A. Zuluaga, A.S. Bosh, S.W. Dieters, P.J. Francis, A.B. Giles, J.G. Greenhill, B. Lade, R. Lucas, D.J. Ramm, Changes in Pluto's atmosphere: 1988–2006. *Astron. J.* **134**, 1–13 (2007). doi:[10.1086/517998](https://doi.org/10.1086/517998)
- G. Fjeldbo, D. Sweetnam, J. Brenkle, E. Christensen, D. Farless, J. Mehta, B. Seidel, W. Michael Jr., A. Wallio, M. Grossi, Viking radio occultation measurements of the Martian atmosphere and topography—Primary mission coverage. *J. Geophys. Res.* **82**, 4317–4324 (1977). doi:[10.1029/JS082i028p04317](https://doi.org/10.1029/JS082i028p04317)
- F. Forget, F. Hourdin, R. Fournier, C. Hourdin, O. Talagrand, M. Collins, S.R. Lewis, P.L. Read, J. Huot, Improved general circulation models of the Martian atmosphere from the surface to above 80 km. *J. Geophys. Res.* **104**, 24155–24176 (1999). doi:[10.1029/1999JE001025](https://doi.org/10.1029/1999JE001025)
- M.P. Golombek, A.F.C. Haldemann, R.A. Simpson, R.L. Fergason, N.E. Putzig, R.E. Arvidson, J.F. Bell III, M.T. Mellon, Martian surface properties from joint analysis of orbital, Earth-based, and surface observations, in *The Martian Surface—Composition, Mineralogy, and Physical Properties*, ed. by J.F. Bell III (Cambridge University Press, Cambridge, 2008), pp. 468–498
- R.M. Haberle, M.A. Kahre, Detecting secular climate change on Mars. *Int. J. Mars Sci. Explor.* **5**, 68–75 (2010). doi:[10.1555/mars.2010.0003](https://doi.org/10.1555/mars.2010.0003)
- R.M. Haberle, M.M. Joshi, J.R. Murphy, J.R. Barnes, J.T. Schofield, G. Wilson, M. Lopez-Valverde, J.L. Hollingsworth, A.F.C. Bridger, J. Schaeffer, General circulation model simulations of the Mars Pathfinder atmospheric structure investigation/meteorology data. *J. Geophys. Res.* **104**, 8957–8974 (1999)
- S.L. Hess, R.M. Henry, C.B. Leovy, J.E. Tillman, J.A. Ryan, Meteorological results from the surface of Mars—Viking 1 and 2. *J. Geophys. Res.* **82**, 4559–4574 (1977). doi:[10.1029/JS082i028p04559](https://doi.org/10.1029/JS082i028p04559)
- S.L. Hess, J.A. Ryan, J.E. Tillman, R.M. Henry, C.B. Leovy, The annual cycle of pressure on Mars measured by Viking landers 1 and 2. *Geophys. Res. Lett.* **7**, 197–200 (1980). doi:[10.1029/GL007i003p00197](https://doi.org/10.1029/GL007i003p00197)
- D.P. Hinson, Radio occultation measurements of pressure variations on Mars, in *Sixth International Conference on Mars*, ed. by A.L. Albee, H.H. Kieffer (2003), p. 3032
- D.P. Hinson, R.A. Simpson, J.D. Twicken, G.L. Tyler, F.M. Flasar, Initial results from radio occultation measurements with Mars Global Surveyor. *J. Geophys. Res.* **104**, 26997–27012 (1999)
- D.P. Hinson, R.A. Simpson, J.D. Twicken, G.L. Tyler, F.M. Flasar, Erratum: Initial results from radio occultation measurements with Mars Global Surveyor. *J. Geophys. Res.* **105**, 1717–1718 (2000)
- D.P. Hinson, M. Pätzold, R.J. Wilson, B. Häusler, S. Tellmann, G.L. Tyler, Radio occultation measurements and MGCM simulations of Kelvin waves on Mars. *Icarus* **193**, 125–138 (2008a). doi:[10.1016/j.icarus.2007.09.009](https://doi.org/10.1016/j.icarus.2007.09.009)
- D.P. Hinson, M. Pätzold, S. Tellmann, B. Häusler, G.L. Tyler, The depth of the convective boundary layer on Mars. *Icarus* **198**, 57–66 (2008b). doi:[10.1016/j.icarus.2008.07.003](https://doi.org/10.1016/j.icarus.2008.07.003)
- J.R. Holton, *An Introduction to Dynamic Meteorology*, 3rd edn. (Academic Press, New York, 1992)
- P.B. James, H.H. Kieffer, D.A. Paige, The seasonal cycle of carbon dioxide on Mars, in *Mars*, ed. by H.H. Kieffer, B.M. Jakosky, C.W. Snyder, M.S. Matthews (University of Arizona Press, Tucson, 1992), pp. 934–968
- Ö. Karatekin, T. Van Hoolst, V. Dehant, Martian global-scale CO<sub>2</sub> exchange from time-variable gravity measurements. *J. Geophys. Res.* **111**, E06003 (2006). doi:[10.1029/2005JE002591](https://doi.org/10.1029/2005JE002591)
- N.J. Kelly, W.V. Boynton, K. Kerry, D. Hamara, D. Janes, R.C. Reedy, K.J. Kim, R.M. Haberle, Seasonal polar carbon dioxide frost on Mars: CO<sub>2</sub> mass and columnar thickness distribution. *J. Geophys. Res.* **111**, E03S07 (2006). doi:[10.1029/2006JE002678](https://doi.org/10.1029/2006JE002678)
- A.J. Kliore, Radio occultation exploration of Mars, in *Exploration of the Planetary System*, ed. by A. Woszczyk, C. Iwaniszewska. IAU Symposium Series, vol. 65 (Reidel, Dordrecht, 1974), pp. 295–316
- A.J. Kliore, Radio occultation observations of the ionospheres of Mars and Venus, in *Venus and Mars: Atmospheres, Ionospheres, and Solar Wind Interactions*. Geophys. Monogr. Ser., vol. 66 (Am. Geophys. Union, Washington, 1992), pp. 265–276
- A.J. Kliore, D.L. Cain, G. Fjeldbo, B.L. Seidel, M.J. Sykes, S.I. Rasool, The atmosphere of Mars from Mariner 9 radio occultation measurements. *Icarus* **17**, 484–516 (1972)
- A.J. Kliore, G. Fjeldbo, B.L. Seidel, M.J. Sykes, P.M. Woiceshyn, S band radio occultation measurements of the atmosphere and topography of Mars from Mariner 9: Extended Mission coverage of polar and intermediate latitudes. *J. Geophys. Res.* **78**, 4331–4351 (1973). doi:[10.1029/JB078i020p04331](https://doi.org/10.1029/JB078i020p04331)

- S.R. Lewis, M. Collins, P.L. Read, F. Forget, F. Hourdin, R. Fournier, C. Hourdin, O. Talagrand, J.-P. Huot, A climate database for Mars. *J. Geophys. Res.* **104**, 24177–24194 (1999). doi:[10.1029/1999JE001024](https://doi.org/10.1029/1999JE001024)
- G.F. Lindal, H.B. Hotz, D.N. Sweetnam, Z. Shippony, J.P. Brenkle, G.V. Hartsell, R.T. Spear, Viking radio occultation measurements of the atmosphere and topography of Mars—Data acquired during 1 martian year of tracking. *J. Geophys. Res.* **84**, 8443–8456 (1979)
- A.S. McEwen, L. Ojha, C. Dundas, S.S. Mattson, S. Byrne, J.J. Wray, S.C. Cull, S.L. Murchie, N. Thomas, V.C. Gulick, Seasonal flows on warm Martian slopes. *Science* **333**, 740–743 (2011)
- M. Pätzold, F.M. Neubauer, L. Carone, A. Hagermann, C. Stanzel, B. Häusler, S. Remus, J. Selle, D. Hagl, D.P. Hinson, R.A. Simpson, G.L. Tyler, S.W. Asmar, W.I. Axford, T. Hagfors, J.-P. Barriot, J.-C. Cerisier, T. Imamura, K.-I. Oyama, P. Janle, G. Kirchengast, V. Dehant, MaRS: Mars Express orbiter radio science (ESA SP-1240: Mars Express: the scientific payload, <http://sci.esa.int/science-e/www/object/index.cfm?fobjectid=34885>, 2004), pp. 141–163
- M. Pätzold, S. Tellmann, B. Häusler, D. Hinson, R. Schaa, G.L. Tyler, A sporadic third layer in the ionosphere of Mars. *Science* **310**, 837–839 (2005). doi:[10.1126/science.1117755](https://doi.org/10.1126/science.1117755)
- S.C.R. Rafkin, R.M. Haberle, T.I. Michaels, The Mars Regional Atmospheric Modeling System: Model description and selected simulations. *Icarus* **151**, 228–256 (2001). doi:[10.1006/icar.2001.6605](https://doi.org/10.1006/icar.2001.6605)
- B.V. Sanchez, D.D. Rowlands, R.M. Haberle, Variations of Mars gravitational field based on the NASA/Ames general circulation model. *J. Geophys. Res.* **111**, E06010 (2006). doi:[10.1029/2005JE002442](https://doi.org/10.1029/2005JE002442)
- A. Seiff, The Viking atmosphere structure experiment—Techniques, instruments, and expected accuracies. *Space Sci. Instrum.* **2**, 381–423 (1976)
- A. Seiff, D.B. Kirk, Structure of the atmosphere of Mars in summer at mid-latitudes. *J. Geophys. Res.* **82**, 4364–4378 (1977)
- A. Seiff, J.E. Tillman, J.R. Murphy, J.T. Schofield, D. Crisp, J.R. Barnes, C. LaBaw, C. Mahoney, J.D. Mihalov, G.R. Wilson, R. Haberle, The atmosphere structure and meteorology instrument on the Mars Pathfinder lander. *J. Geophys. Res.* **102**, 4045–4056 (1997)
- D.E. Smith, M.T. Zuber, G.A. Neumann, Seasonal variations of snow depth on Mars. *Science* **294**, 2141–2146 (2001). doi:[10.1126/science.1066556](https://doi.org/10.1126/science.1066556)
- D.E. Smith, M.T. Zuber, R.M. Haberle, D.D. Rowlands, J.R. Murphy, The Mars seasonal CO<sub>2</sub> cycle and the time variation of the gravity field: A general circulation model simulation. *J. Geophys. Res.* **104**, 1885–1896 (1999). doi:[10.1029/1998JE900024](https://doi.org/10.1029/1998JE900024)
- D.E. Smith, M.T. Zuber, H.V. Frey, J.B. Garvin, J.W. Head, D.O. Muhleman, G.H. Pettengill, R.J. Phillips, S.C. Solomon, H.J. Zwally, W.B. Banerdt, T.C. Duxbury, M.P. Golombek, F.G. Lemoine, G.A. Neumann, D.D. Rowlands, O. Aharonson, P.G. Ford, A.B. Ivanov, C.L. Johnson, P.J. McGovern, J.B. Abshire, R.S. Afzal, X. Sun, Mars Orbiter Laser Altimeter: Experiment summary after the first year of global mapping of Mars. *J. Geophys. Res.* **106**, 23689–23722 (2001). doi:[10.1029/2000JE001364](https://doi.org/10.1029/2000JE001364)
- M.D. Smith, Interannual variability in TES atmospheric observations of Mars during 1999–2003. *Icarus* **167**, 148–165 (2004). doi:[10.1016/S0019-1035\(03\)00287-2](https://doi.org/10.1016/S0019-1035(03)00287-2)
- M.D. Smith, Spacecraft observations of the Martian atmosphere. *Annu. Rev. Earth Planet. Sci.* **36**, 191–219 (2008). doi:[10.1146/annurev.earth.36.031207.124334](https://doi.org/10.1146/annurev.earth.36.031207.124334)
- M.D. Smith, M.J. Wolff, R.T. Clancy, S.L. Murchie, Compact Reconnaissance Imaging Spectrometer observations of water vapor and carbon monoxide. *J. Geophys. Res.* **114**, E00D03 (2009). doi:[10.1029/2008JE003288](https://doi.org/10.1029/2008JE003288)
- J.R. Spencer, J.A. Stansberry, L.M. Trafton, E.F. Young, R.P. Binzel, S.K. Croft, Volatile Transport, seasonal cycles, and atmospheric dynamics on Pluto, in *Pluto and Charon*, ed. by S.A. Stern, D.J. Tholen (1997), pp. 435–473
- S.W. Squyres, R.E. Arvidson, E.T. Baumgartner, J.F. Bell, P.R. Christensen, S. Gorevan, K.E. Herkenhoff, G. Klingelhöfer, M.B. Madsen, R.V. Morris, R. Rieder, R.A. Romero, Athena Mars rover science investigation. *J. Geophys. Res.* **108**, 8062 (2003). doi:[10.1029/2003JE002121](https://doi.org/10.1029/2003JE002121)
- P.A. Taylor, D.C. Catling, M. Daly, C.S. Dickinson, H.P. Gunnlaugsson, A.-M. Harri, C.F. Lange, Temperature, pressure, and wind instrumentation in the Phoenix meteorological package. *J. Geophys. Res.* **113**, E00A10 (2008). doi:[10.1029/2007JE003015](https://doi.org/10.1029/2007JE003015)
- J.E. Tillman, Mars global atmospheric oscillations—Annually synchronized, transient normal-mode oscillations and the triggering of global dust storms. *J. Geophys. Res.* **93**, 9433–9451 (1988). doi:[10.1029/JD093iD08p09433](https://doi.org/10.1029/JD093iD08p09433)
- J.E. Tillman, N.C. Johnson, P. Guttorp, D.B. Percival, The Martian annual atmospheric pressure cycle—Years without great dust storms. *J. Geophys. Res.* **98**, 10963–10971 (1993). doi:[10.1029/93JE01084](https://doi.org/10.1029/93JE01084)
- J.E. Tillman, N.C. Johnson, P. Guttorp, D.B. Percival, Erratum: “The Martian annual atmospheric pressure cycle: Years without great dust storms”. *J. Geophys. Res.* **99**, 3813–3814 (1994). doi:[10.1029/94JE00232](https://doi.org/10.1029/94JE00232)
- E. Van den Acker, T. Van Hoolst, O. de Viron, P. Defraigne, F. Forget, F. Hourdin, V. Dehant, Influence of the seasonal winds and the CO<sub>2</sub> mass exchange between atmosphere and polar caps on Mars’ rotation. *J. Geophys. Res.* **107**, 5055 (2002). doi:[10.1029/2000JE001539](https://doi.org/10.1029/2000JE001539)

- P. Withers, J.R. Barnes, C.G. Justus, H.L. Justh, D.M. Kass, L. Montabone, S.C.R. Rafkin, Comparison of atmospheric observations and predictions for the atmospheric entries of Spirit and Opportunity, in *Lunar and Planetary Institute Science Conference Abstracts*, vol. 39 (2008), p. 2175
- M.H.G. Zhang, J.G. Luhmann, A.J. Kliore, J. Kim, A post-Pioneer Venus reassessment of the martian dayside ionosphere as observed by radio occultation methods. *J. Geophys. Res.* **95**, 14829–14839 (1990)
- R.W. Zurek, J.R. Barnes, R.M. Haberle, J.B. Pollack, J.E. Tillman, C.B. Leovy, Dynamics of the atmosphere of Mars, in *Mars*, ed. by H.H. Kieffer, B.M. Jakosky, C.W. Snyder, M.S. Matthews (University of Arizona Press, Tucson, 1992), pp. 835–933